IEEE Access
Multidisciplinary | Rapid Review | Open Access Journal

Received September 18, 2019, accepted October 8, 2019, date of publication October 15, 2019, date of current version October 28, 2019.

Digital Object Identifier 10.1109/ACCESS.2019.2947637

Cost-Efficient Millimeter Wave Base Station Deployment in Manhattan-Type Geometry

MIAOMIAO DONG[1], (Student Member, IEEE), TAEJOON KIM[2], (Member, IEEE), JINGJIN WU[3], (Member, IEEE), AND ERIC W. M. WONG[1], (Member, IEEE)

[1]Department of Electrical Engineering, City University of Hong Kong, Hong Kong
[2]Department of Electrical Engineering and Computer Science, University of Kansas, Lawrence, KS 66045, USA
[3]Department of Statistics, BNU–HKBU United International College, Zhuhai 519087, China

Corresponding author: Miaomiao Dong (mmdong2-c@my.cityu.edu.hk)

This work was supported in part by the Guangdong University Innovation and Enhancement Programme Funds under Grant 2017KQNCX236.

ABSTRACT Urban millimeter wave (mmWave) communications are limited by link outage due to frequent blockages by obstacles. One approach to this problem is to increase the density of base stations (BSs) to achieve macro diversity gains. Dense BS deployment, however, incurs the increased BS installation cost as well as power consumption. In this work, we propose a framework for connectivity-constrained minimum cost mmWave BS deployment in Manhattan-type geometry (MTG). A closed-form expression of network connectivity is characterized as a function of various factors such as obstacle sizes, BS transmit power, and the densities of obstacles and BSs. Optimization that attains the minimum cost is made possible by incorporating a tight lower bound of the analyzed connectivity expression. A low-complexity algorithm is devised to effectively find an optimal tradeoff between the BS density and transmit power that results in the minimum BS deployment cost while guaranteeing network connectivity. Numerical simulations corroborate our analysis and quantify the best tradeoff of the BS density and transmit power. The proposed BS deployment strategies are evaluated in different network cost configurations, providing useful insights in mmWave network planning and dimensioning.

INDEX TERMS Millimeter wave network, connectivity, base station deployment cost, Manhattan-type geometry, lattice process.

I. INTRODUCTION

Next generation cellular networks will be deployed in millimeter wave (mmWave) bands to support the data-intensive fifth generation (5G) broadband use cases in urban areas [1]–[3]. In mmWave bands, large-scale antenna arrays are used at both base stations (BSs) and user equipments (UEs) to generate directional narrow beams in order to overcome the severe pathloss [4]–[6]. Directional transmission enables almost interference-free communications [7], but it also imposes new challenges, as the weak penetration and diffraction of mmWave propagation make the link susceptible to physical blockages. The blockage incurs frequent link outage in highly-obstructed urban areas. This is in contrast with the conventional sub-6GHz systems, where the outage largely results from co-channel interference rather than a physical blockage.

One approach alleviating mmWave link outage is to cover each UE by multiple BSs, i.e., macro diversity techniques [8], [9]. When a link from a BS is blocked, the UE can switch to another unblocked BS to restore its link. An important practical implication of imposing the macro diversity is an increased number of BSs (i.e., dense BS deployment), which will then increase the expenditures on BS installment. Another alternative is to extend the cell coverage by increasing the transmit power of each BS in order to provide sufficient cell overlap. However, this approach incurs large power consumption. Under a certain connectivity requirement, how to resolve the best tradeoff between the BS density and transmit power that minimizes the BS deployment cost is of great interest for 5G network operators.

Link connectivity is hinged upon network geometry. A Poisson point process (PPP) has been verified to be an

The associate editor coordinating the review of this manuscript and approving it for publication was Zhenyu Xiao.

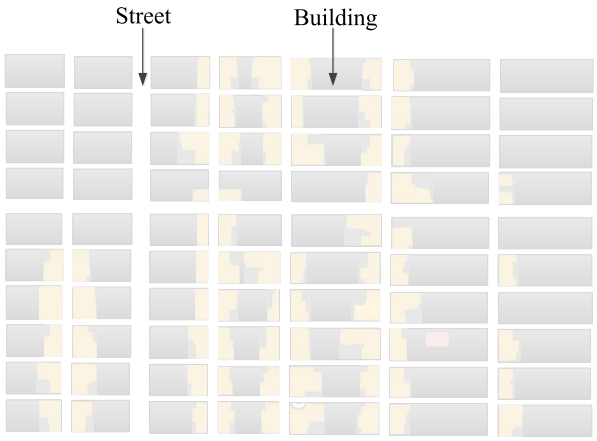

FIGURE 1. An example of the urban MTG.

accurate model in capturing actual urban BS distributions [10], [11]. When characterizing the mmWave links, additional treatment must be given because they are susceptible to physical blockage by urban obstacles. A widely adopted approach in modeling the urban obstacles is the Boolean scheme that assumes the shapes of obstacles are either circles [12], [13] or rectangles [14], [15], and the placement of them follows PPP in stochastic geometry. Under the Boolean scheme, connectivity of urban mmWave networks was previously studied in [8], [9], [12]–[18]. However, these models cannot be extended to analyzing the connectivity of a Manhattan-type geometry (MTG) in Fig. 1, which closely models the urban geometry in most of the scenarios [4], [19]–[23]. Unlike PPP, the obstacles (e.g., buildings) in the MTG are located on grids partitioned by streets.

Ray tracing has been used to evaluate the mmWave link connectivity in MTG [4], [19]. There were attempts to analytically model the MTG based on the random lattice process [21], [22]. In the random lattice process [21], [22], the geometry is partitioned into equidistant horizontal and vertical grids. The occupation of a grid by a random obstacle is independent and identically distributed (i.i.d.) with a certain probability. Based on the lattice process, a connectivity lower bound for the mmWave MTG was analyzed in [23] by incorporating disk-shaped blockage free regions (BFRs), where BFR is an area in which a BS can transmit signals to UEs without blockage. For BS deployment, accurate MTG connectivity analysis is very important. A challenge is that analytically computing accurate connectivity in MTG is prohibitively complex and even impossible [23]. As a remedy, relying on bound analysis relieves the difficulty and makes the underlying task tractable. A previously known connectivity lower bound [23] is rather loose to be used for developing the connectivity-constrained mmWave BS deployment techniques that this work is envisioning. Prior work in this topic mainly focused on conventional sub-6GHz systems [24]–[29], and their connectivity model and the environment are different from those in the mmWave MTG.

In this work, we present a connectivity-constrained minimum cost mmWave BS deployment technique, based on the application of the random lattice process in MTG. We first seek to find tight connectivity lower bounds to be adapted to the formulated optimization problem. The optimized solution resolves the optimal tradeoff between the BS density and transmit power while minimizing BS deployment cost. The resulting BS deployment greatly enhances the connectivity of mmWave networks. Contributions of the work are summarized as follows:

- A new method for connectivity analysis is proposed in the mmWave MTG. The analysis is based on finding a new set of BFRs that directly expresses the network connectivity by exploiting the random lattice process. Then a tractable lower bound of the connectivity probability is provided. The new lower bound greatly improves previous known lower bounds in [23].
- We exploit the connectivity lower bound to formulate and solve a connectivity-constrained optimization problem to achieve the minimum cost BS deployment. We show that the formulated problem can be transformed into a monotonic programming problem. Because conventional monotonic optimization techniques cannot be used due to the out-of-control complexity, we devise a new low-complexity search algorithm that finds a global optimal solution of the problem.
- Numerical simulations verifying the improved performance of the devised algorithm are presented. The results illustrate that the connectivity gaps between the theoretical analysis and the proposed connectivity lower bound within 8%, showing significant improvement over the connectivity analysis in [23], whose lower bound can offset over 20%. We discuss the impacts of various factors, i.e., BS density, transmit power, obstacle density, and obstacle sizes, on the connectivity and evaluate the improved BS deployment results under different cost settings.

The rest of this paper is organized as follows. In Section II, we describe the mmWave network model and assumptions made throughout the paper. The connectivity lower bound of the mmWave MTG is analyzed in Section III. In Section IV, we formulate and solve the connectivity-constrained minimum cost BS deployment problem. Simulation results and conclusions are drawn in Section V and VI, respectively.

II. SYSTEM SETUP

Suppose an urban mmWave network consisting of BSs, UEs, and obstacles (i.e., buildings) in a 2-dimensional MTG. Each UE is associated with one of the surrounding BSs that meets link quality requirement. The associated BS can be in any direction of a UE. After the association, directional link transmission is established. The link can possibly be blocked by obstacles. Outage of a UE occurs when there is no surrounding BS to communicate with. We set an arbitrary point as the origin of the $\mathbb{R}^2$ space and build up the x and y axes to define a coordinate system in the MTG, as shown in Fig. 2.

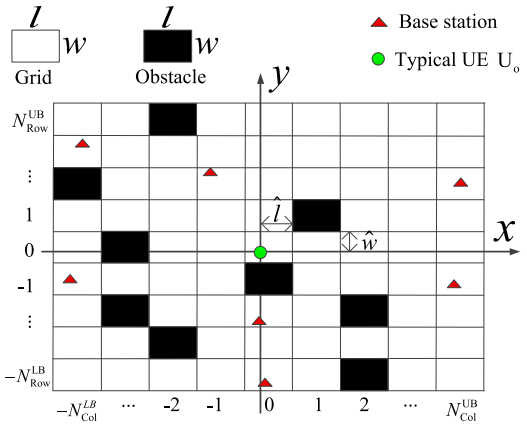

FIGURE 2. Urban mmWave MTG modeled by a random lattice process.

The subsequent analysis and derivations are based on the following assumptions and definitions.

A. OBSTACLES

We assume that obstacles in the MTG in Fig. 2 obey a random lattice process. In the random lattice process, the geometry is partitioned into equidistant horizontal and vertical grids, where the length and width of each gird are set to $l > 0$ and $w > 0$, respectively. Denoting the row grids containing the x axis and the column grids containing the y axis as the 0th row and 0th column, respectively, all rows and columns in Fig. 2 are sequentially labeled from down to up and left to right as $-N^{\mathrm{LB}}_{\mathrm{Row}}, \ldots, 0, \ldots N^{\mathrm{UB}}_{\mathrm{Row}}$ and $-N^{\mathrm{LB}}_{\mathrm{Col}}, \ldots, 0, \ldots N^{\mathrm{UB}}_{\mathrm{Col}}$, respectively. The random lattice process then models the obstacles with length l and width w in urban MTG as illustrated in Fig. 2, where the occupation of each grid by an obstacle is i.i.d. with probability p_o.[1]

Denoting the grid at row a and column b as $\boxdot_{(a,b)}$, we say that occupation state of the grid $\boxdot_{(a,b)}$ becomes $z_{(a,b)} = 1$ if the grid is occupied by an obstacle and $z_{(a,b)} = 0$, otherwise. Hence, the probability that a grid $\boxdot_{(a,b)}$ is occupied by an obstacle is given by

$$\Pr\left(z_{(a,b)} = 1\right) = p_o. \tag{1}$$

Obstacles in the MTG can block mmWave links.

B. BASE STATIONS AND TYPICAL USER EQUIPMENT

The placement of mmWave BSs in MTG obeys a homogeneous PPP $\Phi_{\mathrm{BS}} = \{\mathrm{B}\}$ with density λ, where B represents the location of a particular BS in $\mathbb{R}^2$. We focus on the problem of outdoor mmWave BS deployment, where the outdoor BSs serve the outdoor UEs. Both outdoor BSs and UEs are located in grids that are not occupied by obstacles. All outdoor BSs are assumed to have the same transmit power value P_{Tx} in Watt, where $0 < P_{\mathrm{Tx}} \leq P^{\mathrm{Max}}_{\mathrm{Tx}}$ and $P^{\mathrm{Max}}_{\mathrm{Tx}}$ is the maximum allowed transmit power value.

Connectivity probability of a typical outdoor UE U_o located at the origin in Fig. 2 is a function of parameters l, w, p_o, λ and P_{Tx}, which is denoted as $p_{\mathrm{U}_o}(l, w, p_o, \lambda, P_{\mathrm{Tx}})$. Note that moving the UE U_o (i.e., the origin in $\mathbb{R}^2$) to a different location inside $\boxdot_{(0,0)}$ results in a different connectivity probability. We define $p_c(l, w, p_o, \lambda, P_{\mathrm{Tx}})$ as the minimum connectivity probability among all $\mathrm{U}_o \in \boxdot_{(0,0)}$,

$$p_c(l, w, p_o, \lambda, P_{\mathrm{Tx}}) = \min_{\mathrm{U}_o \in \boxdot_{(0,0)}} p_{\mathrm{U}_o}(l, w, p_o, \lambda, P_{\mathrm{Tx}}). \tag{2}$$

Due to the i.i.d grid occupation statistics and PPP-obeying BS distribution, the value of $p_c(l, w, p_o, \lambda, P_{\mathrm{Tx}})$ is the same over different grids. This being said, without loss of generality, we focus on analyzing connectivity of UEs located at the grid $\boxdot_{(0,0)}$ to achieve the $p_c(l, w, p_o, \lambda, P_{\mathrm{Tx}})$. We shall refer to the minimum connectivity probability $p_c(l, w, p_o, \lambda, P_{\mathrm{Tx}})$ as the network connectivity.

C. LINK BUDGET

An mmWave link is mainly characterized by the line-of-sight (LoS) and a few low-order reflection paths [11], [30]. However, in MTG, the low-order reflection paths have a negligible contribution to the network connectivity because they suffer from much severer attenuation than the LoS path due to additional reflection losses, longer propagation distance, and higher blockage probability [23], [31]. Hence, our focus is given to the connectivity contributed by the major LoS components, while neglecting minor reflection components.

For an LoS link with length r meters, we adopt the pathloss model at 28 GHz [31]

$$PL(r) = 61.4 + 21\log_{10}(r) \text{ in dB}.$$

The received power at the UE U_o can be given by

$$P_{\mathrm{Rx}} = f(P_{\mathrm{Tx}}, r) = P_{\mathrm{Tx}} G_{\mathrm{Tx}} G_{\mathrm{Rx}} 10^{-PL(r)/10}, \tag{3}$$

where G_{Tx} and G_{Rx} are directional beam gains at the BS and UE, respectively. We let P_{Th} be the minimum power required at the receiver for successful signal detection. Setting $P_{\mathrm{Rx}} = P_{\mathrm{Th}}$ in (3) allows us to get the BS coverage radius

$$R = f^{-1}(P_{\mathrm{Tx}}, P_{\mathrm{Th}}), \tag{4}$$

whose maximum value $R^{\mathrm{Max}} = f^{-1}(P^{\mathrm{Max}}_{\mathrm{Tx}}, P_{\mathrm{Th}})$.

D. BLOCKAGE FREE REGION (BFR)

If there exists an outdoor BS $\mathrm{B} \in \Phi_{\mathrm{BS}}$ that can serve the UE U_o, we say that B is in the BFR Ψ of the U_o, namely, $\mathrm{B} \in \Psi$. This means any $\mathrm{B} \in \Psi$ simultaneously satisfies two conditions: (i) B is located in the disk with radius R in (4), that is,

$$\mathcal{O}(R) = \left\{\mathrm{X} | L_{\overline{\mathrm{U}_o\mathrm{X}}} \leq R\right\}, \tag{5}$$

where $L_{\overline{\mathrm{U}_o\mathrm{X}}}$ represents the length of the LoS segment $\overline{\mathrm{U}_o\mathrm{X}}$ connecting points U_o and X, and (ii) $\overline{\mathrm{U}_o\mathrm{B}}$ is not blocked by

[1]For ease of presentation, all grids in the MTG are assumed to have the same size and occupation probability p_o. Extension of the model to the cases where grids have different sizes and occupation probabilities is straightforward. One can also emulate more practical scenarios. For example, setting occupation probability to $p_o = 0$ of the grids in a same row or column represent a street. A practical scenario is actually a realization of the random lattice process in Fig. 2.

any obstacle. Defining the region occupied by obstacles as $\mathcal{A}=\left\{\boxdot_{(a,b)}|z_{(a,b)}=1,\forall a,b\right\}$, the condition (ii) is equivalent to

$$\mathrm{B}\in\mathcal{F}=\left\{\mathrm{X}|\overline{\mathrm{U}_o\mathrm{X}}\cap\mathcal{A}=\emptyset\right\}.$$

Therefore, the BFR Ψ can be formally defined by

$$\Psi=\mathcal{O}(R)\cap\mathcal{F}. \tag{6}$$

Since $\Psi\subset\mathcal{O}(R)$, only BSs located in $\mathcal{O}(R)$ can contribute to the connectivity of UE U_o. Hence, in Fig. 2, we focus on the region consisting of grids $\boxdot_{(a,b)}$ for

$$a\in\left[-N_{\mathrm{Row}}^{\mathrm{LB}},N_{\mathrm{Row}}^{\mathrm{UB}}\right],\quad b\in\left[-N_{\mathrm{Col}}^{\mathrm{LB}},N_{\mathrm{Col}}^{\mathrm{UB}}\right], \tag{7}$$

where $\left[-N_{\mathrm{Row}}^{\mathrm{LB}},N_{\mathrm{Row}}^{\mathrm{UB}}\right]$ (respectively, $\left[-N_{\mathrm{Col}}^{\mathrm{LB}},N_{\mathrm{Col}}^{\mathrm{UB}}\right]$) contains the integers from $-N_{\mathrm{Row}}^{\mathrm{LB}}$ to $N_{\mathrm{Row}}^{\mathrm{UB}}$ (resp. from $-N_{\mathrm{Col}}^{\mathrm{LB}}$ to $N_{\mathrm{Col}}^{\mathrm{UB}}$), and

$$N_{\mathrm{Row}}^{\mathrm{LB}}=\left\lceil\frac{R-(w-\hat{w})}{w}\right\rceil,\quad N_{\mathrm{Row}}^{\mathrm{UB}}=\left\lceil\frac{R-\hat{w}}{w}\right\rceil,$$
$$N_{\mathrm{Col}}^{\mathrm{LB}}=\left\lceil\frac{R-(l-\hat{l})}{l}\right\rceil,\quad N_{\mathrm{Col}}^{\mathrm{UB}}=\left\lceil\frac{R-\hat{l}}{l}\right\rceil, \tag{8}$$

where $\lceil x\rceil$ represents the minimum integer that is greater than or equal to x, and $\hat{l}$ and $\hat{w}$, as shown in Fig. 2, are the length and width of the sub-rectangle of $\boxdot_{(0,0)}$ in orthant 1. The $\boxdot_{(a,b)}$s for $a\in\left[-N_{\mathrm{Row}}^{\mathrm{LB}},N_{\mathrm{Row}}^{\mathrm{UB}}\right]$ and $b\in\left[-N_{\mathrm{Col}}^{\mathrm{LB}},N_{\mathrm{Col}}^{\mathrm{UB}}\right]$ constitute a rectangle circumscribing the disk $\mathcal{O}(R)$ in (5).

III. CONNECTIVITY ANALYSIS

The outdoor UE U_o in Fig. 2 is in connectivity when there are BSs in the BFR Ψ in (6), i.e., $\Psi\cap\Phi_{\mathrm{BS}}\neq\emptyset$. Hence the $p_{\mathrm{U}_o}(l,w,p_o,\lambda,P_{\mathrm{Tx}})$ in (2) can be expressed as

$$p_{\mathrm{U}_o}(l,w,p_o,\lambda,P_{\mathrm{Tx}})=\Pr(\Psi\cap\Phi_{\mathrm{BS}}\neq\emptyset). \tag{9}$$

The goal of this section is to derive a tight lower bound of the $p_{\mathrm{U}_o}(l,w,p_o,\lambda,P_{\mathrm{Tx}})$ that admits a computationally feasible closed-form expression. Throughout this section, we shall use p_{U_o} to denote $p_{\mathrm{U}_o}(l,w,p_o,\lambda,P_{\mathrm{Tx}})$ for simplicity. Because connectivity probability of the outdoor UE $\mathrm{U}_o\in\boxdot_{(0,0)}$ is the focus, we hold $z_{(0,0)}=0$.

A. CONNECTIVITY PROBABILITY

Seen from Fig. 2, the MTG is divided into four orthants by the x and y axes. We name anticlockwise the orthants as orthant 1, 2, 3, and 4, where orthant 1 is outlined by the semi-positive x axis and y axis. The UE U_o is in connectivity when it can be served by an outdoor BS in any of the four orthants. The first step of our method is to analyze the counterparts of the Ψ and Φ_{BS} in each orthant i, i.e., $\Psi^{(i)}$ and $\Phi_{\mathrm{BS}}^{(i)}$, respectively. The connectivity p_{U_o} in (9) is obtained as

$$p_{\mathrm{U}_o}=1-\Pr\left(\bigcap_{i=1}^{4}\left(\Psi^{(i)}\cap\Phi_{\mathrm{BS}}^{(i)}=\emptyset\right)\right). \tag{10}$$

We note in Fig. 3 that the occupation state of a grid at row 0 or column 0 can simultaneously affect the BFR $\Psi^{(i)}$ of two

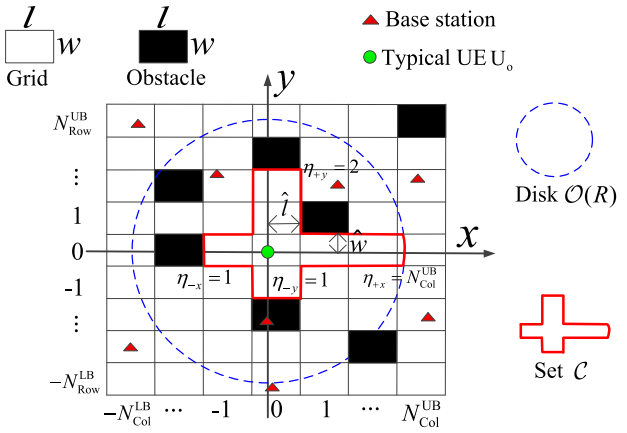

FIGURE 3. Illustration of the set $\mathcal{C}$ in (11) in a random lattice modeled MTG.

orthants. This implies that the connectivity of an orthant is correlated with the connectivity of other orthants, which inflicts difficulty in computing (10).

To decouple the correlation, we denote points of the BFR Ψ at the row 0 or column 0 as

$$\mathcal{C}=\Psi\cap\left\{\mathrm{X}\in\boxdot_{(0,b)}\cup\boxdot_{(a,0)},\quad\forall a\in[-N_{\mathrm{Row}}^{\mathrm{LB}},N_{\mathrm{Row}}^{\mathrm{UB}}],\right.$$
$$\left.\forall b\in[-N_{\mathrm{Col}}^{\mathrm{UB}},N_{\mathrm{Col}}^{\mathrm{UB}}]\right\}, \tag{11}$$

which varies with the occupation states of grids at row 0 and column 0, as exemplified in Fig. 3. Conditioned on a realization of $\mathcal{C}$, the $\Psi^{(i)}$ for $i\in[1,4]$ become into mutually independent. The independence leads to the p_{U_o} in (10) conditioned on the jth realization of $\mathcal{C}$, denoted by $\mathcal{C}_j$, as

$$p_{\mathrm{U}_o|\mathcal{C}_j}=1-\prod_{i=1}^{4}\Pr\left(\Psi^{(i)}\cap\Phi_{\mathrm{BS}}^{(i)}=\emptyset|\mathcal{C}_j\right)$$
$$=1-\prod_{i=1}^{4}\left(1-p_{\mathrm{U}_o|\mathcal{C}_j}^{(i)}\right), \tag{12}$$

where $p_{\mathrm{U}_o|\mathcal{C}_j}^{(i)}=\Pr(\Psi^{(i)}\cap\Phi_{\mathrm{BS}}^{(i)}\neq\emptyset|\mathcal{C}_j)$. The connectivity probability p_{U_o} in (10) over random $\mathcal{C}$ is thus given by

$$p_{\mathrm{U}_o}=E_{\mathcal{C}}[p_{\mathrm{U}_o|\mathcal{C}}]=\sum_{j=1}^{J}\left(1-\prod_{i=1}^{4}\left(1-p_{\mathrm{U}_o|\mathcal{C}_j}^{(i)}\right)\right)\Pr\left(\mathcal{C}_j\right), \tag{13}$$

where $E_{\mathcal{C}}[p_{\mathrm{U}_o|\mathcal{C}}]$ is the expectation of $p_{\mathrm{U}_o|\mathcal{C}}$ in terms of $\mathcal{C}$, and J is the number of realizations of the $\mathcal{C}$ in (11). In each realization of the obstacle distribution, we compute four variables based on the obstacle occupation states of grids on the four semi-x and -y axes,

$$\eta_{+y}=\max_{q\in[0,N_{\mathrm{Row}}^{\mathrm{UB}}]}q\quad\text{s.t.}\sum_{a=0}^{q}z_{(a,0)}=0, \tag{14}$$

$$\eta_{+x}=\max_{q\in[0,N_{\mathrm{Col}}^{\mathrm{UB}}]}q\quad\text{s.t.}\sum_{b=0}^{q}z_{(0,b)}=0, \tag{15}$$

$$\eta_{-y} = \max_{q\in[-N_{\text{Row}}^{\text{LB}},0]} |q| \quad \text{s.t.} \sum_{a=q}^{0} z_{(a,0)} = 0, \tag{16}$$

$$\eta_{-x} = \max_{q\in[-N_{\text{Col}}^{\text{LB}},0]} |q| \quad \text{s.t.} \sum_{b=q}^{0} z_{(0,b)} = 0. \tag{17}$$

Seen from Fig. 3, the $\mathcal{C}$ is uniquely determined by the set $\{\eta_{+y}, \eta_{+x}, \eta_{-y}, \eta_{-x}\}$, and vice versa. Since the four variables $\eta_{+y}, \eta_{+x}, \eta_{-y}$ and η_{-x} are mutually indepednent, the J in (13) is computed as

$$J = (N_{\text{Row}}^{\text{LB}} + 1)(N_{\text{Row}}^{\text{UB}} + 1)(N_{\text{Col}}^{\text{LB}} + 1)(N_{\text{Col}}^{\text{UB}} + 1), \tag{18}$$

and the probability $\Pr(\mathcal{C}_j)$ in (13) is given by

$$\Pr(\mathcal{C}) = \prod_{i\in\{+x,+y,-y,-x\}} \Pr(\eta_i),$$

where $\Pr(\eta_i), \forall i$ are computed using the same approach. For instance, we have

$$\Pr(\eta_{+y}) = \begin{cases} (1-p_o)^{\eta_{+y}} p_o, & \text{if} \quad \eta_{+y} < N_{\text{Row}}^{\text{UB}} \\ (1-p_o)^{\eta_{+y}}, & \text{if} \quad \eta_{+y} = N_{\text{Row}}^{\text{UB}}, \end{cases} \tag{19}$$

where $(1-p_o)^{\eta_{+y}}$ is the probability that grids $\boxdot_{(a,0)}$ for $a \in [1, \eta_{+y}]$ are not occupied by obstacles.

Finding the p_{U_o} in (13) needs the closed-from expression of $p_{\text{U}_o|\mathcal{C}_j}^{(i)}, j \in [1, J], i \in [1, 4]$. In what follows, we focus on the computation of $p_{\text{U}_o|\mathcal{C}_j}^{(1)}, j \in [1, J]$, keeping in mind that the exactly same approach can be applied to the calculations of $p_{\text{U}_o|\mathcal{C}_j}^{(i)}, i \in [2, 4]$.

B. CONNECTIVITY PROBABILITY IN ORTHANT 1

Without loss of generality, we focus on an arbitrary realization $\mathcal{C}_j \in \mathcal{C}$ in (11). The subscript j of $p_{\text{U}_o|\mathcal{C}_j}^{(1)}$ in (12) is omitted whenever there is no ambiguity.

In Fig. 2, conditioned on a realization of $\mathcal{C}$, the connectivity in orthant 1 is characterized by the occupation state set

$$\mathcal{D} = \left\{ z_{(a,b)},\ a \in [1, N_{\text{Row}}^{\text{UB}}], b \in [1, N_{\text{Col}}^{\text{UB}}] \right\}. \tag{20}$$

Under different realization of $\mathcal{D}$, we can obtain different $\Psi^{(1)}$. This allows us to express the $p_{\text{U}_o|\mathcal{C}}^{(1)}$ as

$$\begin{aligned} p_{\text{U}_o|\mathcal{C}}^{(1)} &= \Pr\left(\Psi^{(1)} \cap \Phi_{\text{BS}}^{(1)} \neq \emptyset | \mathcal{C}\right) \\ &\overset{(a)}{=} E_{\Psi^{(1)}}\left[1 - e^{-\lambda S\left(\Psi^{(1)}\right)} | \Psi^{(1)}, \mathcal{C}\right] \\ &= \sum_{m} \left(1 - e^{-\lambda S\left(\Psi_{m|\mathcal{C}}^{(1)}\right)}\right) \Pr\left(\Psi_{m|\mathcal{C}}^{(1)}\right), \end{aligned} \tag{21}$$

where (a) is because, for PPP-distributed BSs, the probability that there are BSs in a $\Psi^{(1)}$ (i.e., $\Psi^{(1)} \cap \Phi_{\text{BS}}^{(1)} \neq \emptyset$) is given by $1 - \exp\left(-\lambda S(\Psi^{(1)})\right)$, in which $S(\Psi^{(1)})$ is the area of $\Psi^{(1)}$. The $\Psi_{m|\mathcal{C}}^{(1)}$ in (21) is the mth instance of $\Psi^{(1)}$ conditioned on $\mathcal{C}$. In (21), one should find the $S(\Psi_{m|\mathcal{C}}^{(1)})$ for every m. According to definition of the BFR in (6), each $\Psi_{m|\mathcal{C}}^{(1)}$ has an irregular shape, as shown in Fig. 4, making computation of its area challenging.

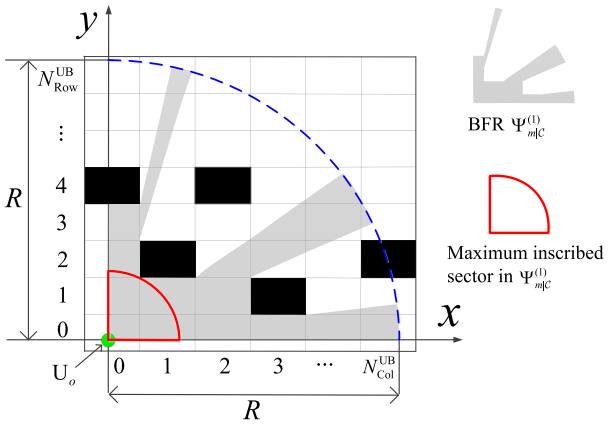

FIGURE 4. A $\Psi_{m|\mathcal{C}}^{(1)}$ in (21) and its maximum inscribed sector.

To circumvent the difficulty, we alternatively derive a tractable lower bound of the $p_{\text{U}_o|\mathcal{C}}^{(1)}$ in (21) by finding a tractable BFR set $\{\Omega_{t|\mathcal{C}}^{(1)}\}_{t=1}^{T}$ with T elements satisfying three conditions: (i) $S\left(\Omega_{t|\mathcal{C}}^{(1)}\right)$ for every $t \in [1, T]$ is known, (ii) each $\Psi_{m|\mathcal{C}}^{(1)}$ can find a maximum inscribed BFR from $\{\Omega_{t|\mathcal{C}}^{(1)}\}_{t=1}^{T}$, i.e.,

$$\Omega_{t_m|\mathcal{C}}^{(1)} = \max_{\Omega_{t|\mathcal{C}}^{(1)} \subset \Psi_{m|\mathcal{C}}^{(1)},\ t\in[1,T]} S\left(\Omega_{t|\mathcal{C}}^{(1)}\right), \tag{22}$$

and (iii) each $\Omega_{t|\mathcal{C}}^{(1)}$ is the maximum inscribed BFR of a $\Psi_{m|\mathcal{C}}^{(1)}$. Because of $S\left(\Psi_{m|\mathcal{C}}^{(1)}\right) \geq S\left(\Omega_{t_m|\mathcal{C}}^{(1)}\right)$, a lower bound of the $p_{\text{U}_o|\mathcal{C}}^{(1)}$ in (21) is given by

$$\begin{aligned} p_{\text{U}_o|\mathcal{C}}^{(1)} \geq \bar{p}_{\text{U}_o|\mathcal{C}}^{(1)} &= \sum_{m} \left(1 - e^{-\lambda S\left(\Omega_{t_m|\mathcal{C}}^{(1)}\right)}\right) \Pr\left(\Psi_{m|\mathcal{C}}^{(1)}\right) \\ &\overset{(b)}{=} \sum_{t=1}^{T} \left(1 - e^{-\lambda S\left(\Omega_{t|\mathcal{C}}^{(1)}\right)}\right) \Pr\left(\Omega_{t|\mathcal{C}}^{(1)}\right), \end{aligned} \tag{23}$$

where (b) is because of the condition (iii), and

$$\Pr\left(\Omega_{t|\mathcal{C}}^{(1)}\right) = \sum_{m\in\mathcal{M}_t} \Pr\left(\Psi_{m|\mathcal{C}}^{(1)}\right)$$

in which $\mathcal{M}_t$ is the index set of $\Psi_{m|\mathcal{C}}^{(1)}$s who have the same maximum inscribed BFR $\Omega_{t|\mathcal{C}}^{(1)}$. Obviously, tightness of the lower bound in (23) is guaranteed if each $\Psi_{m|\mathcal{C}}^{(1)}$ is accurately approximated by its maximum inscribed BFR. This requires the BFR set $\{\Omega_{t|\mathcal{C}}^{(1)}\}_{t=1}^{T}$ contains large number of elements with various shapes.

Referring to [23, (8)], a simple method finding the $\{\Omega_{t|\mathcal{C}}^{(1)}\}_{t=1}^{T}$ is to set each $\Omega_{t|\mathcal{C}}^{(1)}$ to be the subregion of a disk $\mathcal{O}(r)$ in orthant 1 (i.e., sector-shaped $\Omega_{t|\mathcal{C}}^{(1)}$), where r is a discrete random variable. The sector-shaped $\{\Omega_{t|\mathcal{C}}^{(1)}\}_{t=1}^{T}$ will lead to a loose lower bound in (23) because the shape of each $\Psi_{m|\mathcal{C}}^{(1)}$ is usually far from its sector-shaped approximation. For instance in Fig. 4, the maximum inscribed sector in a $\Psi_{m|\mathcal{C}}^{(1)}$ is much smaller than the $\Psi_{m|\mathcal{C}}^{(1)}$ in area. To obtain a relatively tight lower bound in (23), we find a new BFR set $\{\Omega_{t|\mathcal{C}}^{(1)}\}_{t=1}^{T}$ in the next subsection.

C. A NEW TRACTABLE BFR SET IN ORTHANT 1

As observed from Fig. 3, the $\Psi^{(1)}_{m|\mathcal{C}}$ in (23) for all m have a common region, denoted by $\mathcal{C}^{(1)}$, which is the subregion of the $\mathcal{C}$ overlapped with orthant 1. Inside the $\mathcal{C}^{(1)}$, a tractable subregion $\overline{\mathcal{C}}^{(1)}$ is derived to be the common region of the targeted $\{\Omega^{(1)}_{t|\mathcal{C}}\}_{t=1}^{T}$. As in Fig. 3, the $\mathcal{C}^{(1)}$ is L-shaped and is determined by the η_{+y} in (14) and η_{+x} in (15). When $\eta_{+y} < N^{\text{UB}}_{\text{Row}}$ and $\eta_{+x} < N^{\text{UB}}_{\text{Col}}$, the $\mathcal{C}^{(1)}$ is limited by occupation states of grids and has regular shape. The $\overline{\mathcal{C}}^{(1)}$ can be directly set to $\overline{\mathcal{C}}^{(1)} = \mathcal{C}^{(1)}$ whose area

$$S(\overline{\mathcal{C}}^{(1)}) = \hat{l}\left(\hat{w} + w\eta_{+y}\right) + \hat{w}\left(\hat{l} + l\eta_{+x}\right). \tag{24}$$

When $\eta_{+y} = N^{\text{UB}}_{\text{Row}}$ and/or $\eta_{+x} = N^{\text{UB}}_{\text{Col}}$ in Fig. 3, part of the $\boxdot_{(\eta_{+y},0)}$ and/or $\boxdot_{(0,\eta_{+x})}$ is in the $\mathcal{C}^{(1)}$, leading to irregular shape of $\mathcal{C}^{(1)}$. In this case, the $\overline{\mathcal{C}}^{(1)}$ is set to be the $\mathcal{C}^{(1)}$ excluding the part of the $\boxdot_{(\eta_{+y},0)}$ and/or $\boxdot_{(0,\eta_{+x})}$. We can compute the $S(\overline{\mathcal{C}}^{(1)})$ using (24) by updating $\eta_{+y} = \eta_{+y} - 1$ and/or $\eta_{+x} = \eta_{+x} - 1$.

Finding the BFR set $\{\Omega^{(1)}_{t|\mathcal{C}}\}_{t=1}^{T}$ is now of interest. For ease of computing $S\left(\Omega^{(1)}_{t|\mathcal{C}}\right) - S(\overline{\mathcal{C}}^{(1)})$, we consider each $\Omega^{(1)}_{t|\mathcal{C}}$ consists of a rectangular region at each column $b \in [1, \eta_{+x}]$ and tractably express it in the form

$$\Omega^{(1)}_{t|\mathcal{C}} = \overline{\mathcal{C}}^{(1)} + \underbrace{\sum_{a=1}^{n^{(1)}_1} \boxdot_{(a,1)}}_{\text{column 1}} + \ldots + \underbrace{\sum_{a=1}^{n^{(1)}_{\eta_{+x}}} \boxdot_{(a,\eta_{+x})}}_{\text{column } \eta_{+x}}, \tag{25}$$

where $n^{(1)}_b$ for $b \in [1, \eta_{+x}]$ is a row index satisfying

$$\begin{cases} n^{(1)}_b \le \alpha^{(1)}_b = \max\limits_{q \in [0, N^{\text{UB}}_{\text{Col}}]} q \quad \text{subject to } \sum_{b=0}^{q} \boxdot_{(0,b)} \subset \mathcal{O}(R) \\ n^{(1)}_b \le n^{(1)}_{b-1}, \quad \text{where } n^{(1)}_0 = \eta_{+y} \text{ in.(14)} \end{cases} \tag{26}$$

In (26), the $n^{(1)}_b \le \alpha^{(1)}_b$ guarantees the obtained $\Omega^{(1)}_{t|\mathcal{C}} \subset \mathcal{O}(R)$. The $n^{(1)}_b \le n^{(1)}_{b-1}$, as illustrated in Fig. 5, ensures the $\Omega^{(1)}_{t|\mathcal{C}} \subset \mathcal{F}$ in (6) if there is no obstacle in the $\Omega^{(1)}_{t|\mathcal{C}}$. Hence, the $\Omega^{(1)}_{t|\mathcal{C}}$ in (25) can be a BFR defined in (6).

Each $\Omega^{(1)}_{t|\mathcal{C}}$ in (25) is uniquely determined by the set

$$\mathcal{N}^{(1)} = \left\{n^{(1)}_0 = \eta_{+y},\ n^{(1)}_1, n^{(1)}_2, \ldots, n^{(1)}_{\eta_{+x}}\right\}. \tag{27}$$

with the element domain (26), i.e.,

$$n^{(1)}_b \in \left[0, \min\left(\alpha^{(1)}_b, n^{(1)}_{b-1}\right)\right], \quad \forall b \in [1, \eta_{+x}]. \tag{28}$$

By enumerating the $\mathcal{N}^{(1)}$, we obtain a BFR set $\{\Omega^{(1)}_{t|\mathcal{C}}\}_{t=1}^{T}$.

D. CONNECTIVITY LOWER BOUND

To use the obtained $\{\Omega^{(1)}_{t|\mathcal{C}}\}_{t=1}^{T}$ to compute the lower bound in (23), we first show that the $\{\Omega^{(1)}_{t|\mathcal{C}}\}_{t=1}^{T}$ satisfies the three conditions specified above (23). According to (25), the area

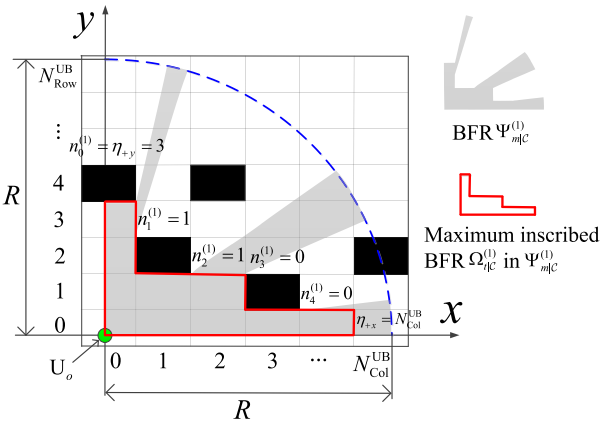

FIGURE 5. A $\Psi_{m|\mathcal{C}}$ in (21) and its maximum inscribed $\Omega^{(1)}_{t|\mathcal{C}}$ in (25).

$S\left(\Omega^{(1)}_{t|\mathcal{C}}\right) = S(\overline{\mathcal{C}}^{(1)}) + \sum_{b=1}^{\eta_{+x}} lwn^{(1)}_b$. Since a $\Omega^{(1)}_{t|\mathcal{C}} = \overline{\mathcal{C}}^{(1)}$ in (25) obtained by

$$\mathcal{N}^{(1)} = \left\{n^{(1)}_0 = \eta_{+y},\ n^{(1)}_1 = 0, n^{(1)}_2 = 0, \ldots, n^{(1)}_{\eta_{+x}} = 0\right\}$$

is the common region of all instances $\Psi^{(1)}_{m|\mathcal{C}}$ in (21), each $\Psi^{(1)}_{m|\mathcal{C}}$ can find a maximum inscribed BFR in $\{\Omega^{(1)}_{t|\mathcal{C}}\}_{t=1}^{T}$ by using (22). Seen from Fig. 5, setting occupation states of grids crossed and overlapped with a $\Omega^{(1)}_{t|\mathcal{C}}$ to be 0s and occupation states of the remaining grids in the MTG to be 1s, we obtain a $\Psi^{(1)}_{m|\mathcal{C}}$ whose maximum inscribed BFR must be the $\Omega^{(1)}_{t|\mathcal{C}}$. We can then compute the lower bound in (23) as

$$\overline{p}^{(1)}_{\text{U}_o|\mathcal{C}} = \sum_{n^{(1)}_1=0}^{\min\left(\alpha^{(1)}_1, n^{(1)}_0\right)} \sum_{n^{(1)}_2=0}^{\min\left(\alpha^{(1)}_2, n^{(1)}_1\right)} \cdots \sum_{n^{(1)}_{\eta_{+x}}=0}^{\min\left(\alpha^{(1)}_{\eta_{+x}}, n^{(1)}_{\eta_{+x}-1}\right)} \left(1 - e^{-\lambda S\left(\Omega^{(1)}_{t|\mathcal{C}}\right)}\right) \Pr\left(\mathcal{N}^{(1)}_t\right), \tag{29}$$

where $\Pr\left(\mathcal{N}^{(1)}_t\right)$ follows Lemma 1. Using the same approach, we define $\mathcal{N}^{(i)}$ for $i \in [2, 4]$ and find $\overline{p}^{(i)}_{\text{U}_o|\mathcal{C}}$ for each $i \in [1, 4]$ to compute the lower bound of p_{U_o} in (13) as

$$\overline{p}_{\text{U}_o} = \sum_{j=1}^{J} \left(1 - \prod_{i=1}^{4} \left(1 - \overline{p}^{(i)}_{\text{U}_o|\mathcal{C}_j}\right)\right) \Pr\left(\mathcal{C}_j\right). \tag{30}$$

Lemma 1: Probability of a realization of $\mathcal{N}^{(1)}$ is computed as

$$\Pr\left(\mathcal{N}^{(1)}\right) = \prod_{b=1}^{\eta_{+x}} \Pr\left(n^{(1)}_b | n^{(1)}_{b-1}\right), \tag{31}$$

where $\Pr\left(n^{(1)}_b | n^{(1)}_{b-1}\right)$ is the probability that $n^{(1)}_b$ is selected from its domain (28) determined by $n^{(1)}_{b-1}$ and

$$\Pr\left(n^{(1)}_b | n^{(1)}_{b-1}\right) = \begin{cases} (1-p_o)^{n^{(1)}_b} p_o, & \text{if } n^{(1)}_b < \min\left(\alpha^{(1)}_b, n^{(1)}_{b-1}\right) \\ (1-p_o)^{n^{(1)}_b}, & \text{if } n^{(1)}_b = \min\left(\alpha^{(1)}_b, n^{(1)}_{b-1}\right). \end{cases} \tag{32}$$

Proof: See the Appendix. ■

Remark 1: Different realizations of $\mathcal{N}^{(1)}$ in (27) yield BFR $\Omega^{(1)}_{t|\mathcal{C}}$s in (25) with different shapes. Compared to the sector-shaped $\{\Omega^{(1)}_{t|\mathcal{C}}\}^T_{t=1}$, as illustrated in Fig. 4 and 5, the derived $\{\Omega^{(1)}_{t|\mathcal{C}}\}^T_{t=1}$ can approximate instances of $\Psi^{(1)}$ in (23) in a more accurate way. Hence, we can obtain a relatively tight connectivity lower bound, as can be seen in Section V.

Remark 2: When computing the $\overline{p}_{U_o}$ in (30), we first use the BS coverage radius R to determine the N^{LB}_{Row}, N^{UB}_{Row}, N^{LB}_{Col}, and N^{UB}_{Col} in (8), and the $\alpha^{(i)}_b$s in (26) for different b and $i \in [1, 4]$. These variables are all integers and used to determine the $\overline{p}_{U_o}$. Hence, the $\overline{p}_{U_o}$ is an implicit function of R.

IV. BASE STATION DEPLOYMENT PROBLEM

We find the location of $U_o \in \boxdot_{(0,0)}$ in Fig. 2 that has the minimum $\overline{p}_{U_o}(l, w, p_o, \lambda, R)$ in (30), where $R = f^{-1}(P_{\mathrm{Tx}}, P_{\mathrm{Th}})$ in (4). According to (2), the $\overline{p}_{U_o}(l, w, p_o, \lambda, R)$ at this U_o location is a lower bound of the network connectivity $p_c(l, w, p_o, \lambda, R)$, denoted by $\overline{p}_c(l, w, p_o, \lambda, R)$. In this section, we use $\overline{p}_c(l, w, p_o, \lambda, R)$ to construct the network connectivity constraint and then formulate and solve the minimum cost BS deployment problem in the mmWave MTG.

A. PROBLEM FORMULATION

We first define the objective function. Based on the properties of PPP, the average number of outdoor BSs per square meter and the power consumption at these BSs are given by $\lambda(1 - p_o)$ and $(P_{\mathrm{Tx}} + P_{\mathrm{C}})\lambda(1 - p_o)$, respectively, where P_{Tx} is the transmit power and P_{C} is the constant circuit power at each BS [32]. Let c_{BS} be the cost of installing an outdoor BS and c_{Pw} be the cost of unit power in a certain period.[2] The average BS deployment cost per square meter is given by

$$\lambda(1-p_o)\big(c_{\mathrm{BS}} + c_{\mathrm{Pw}}(P_{\mathrm{Tx}}+P_{\mathrm{C}})\big).$$

With the minimum required network connectivity ζ_{Con}, the connectivity-constrained minimum cost BS deployment problem is formulated as

$$\min_{\lambda, P_{\mathrm{Tx}}} \ \lambda(1-p_o)\big(c_{\mathrm{BS}} + c_{\mathrm{Pw}}(P_{\mathrm{Tx}} + P_{\mathrm{C}})\big) \tag{33}$$

$$\text{s.t. } \overline{p}_c(l, w, p_o, \lambda, R) \geq \zeta_{\mathrm{Con}}, \tag{34}$$

$$R = f^{-1}(P_{\mathrm{Tx}}, P_{\mathrm{Th}}),$$

$$\lambda > 0, \quad 0 < P_{\mathrm{Tx}} \leq P^{\mathrm{Max}}_{\mathrm{Tx}},$$

where λ and P_{Tx} are decision variables, while geometry parameters l, w, and p_o are fixed at this stage. It is verified from the definition of the objective function in (33) and derivations of the network connectivity $\overline{p}_c(l, w, p_o, \lambda, R)$ (i.e., $\overline{p}_{U_o}(l, w, p_o, \lambda, R)$ in (30)) that the objective function and $\overline{p}_c(l, w, p_o, \lambda, R)$ in problem (33) are both monotonically increasing with respect to the BS density λ and transmit power P_{Tx}. These can be intuitively known since high BS density and large BS coverage radius contribute to the network connectivity performance, but incurs higher cost. Hence, problem (33) is monotonic optimization programming. Based on the monotonicity, we derive Lemma 2.

Lemma 2: The optimal solution $(\lambda^\star, P^\star_{Tx})$ of problem (33) guarantees the equality $\overline{p}_c(l, w, p_o, \lambda^\star, R^\star) = \zeta_{Con}$ in (34), where $R^\star = f^{-1}(P^\star_{Tx}, P_{Th})$.

Proof: We prove the lemma by contradiction. If

$$\overline{p}_c\left(l, w, p_o, \lambda^\star, R^\star\right) > \zeta_{\mathrm{Con}},$$

we fix $P^\star_{\mathrm{Tx}}$ and reduce $\lambda^\star$ to λ_1 so that $\overline{p}_c(l, w, p_o, \lambda_1, R^\star) = \zeta_{\mathrm{Con}}$. It is clear that the feasible solution $(\lambda_1, P^\star_{\mathrm{Tx}})$ yields a smaller objective value than that of $(\lambda^\star, P^\star_{\mathrm{Tx}})$. This contradicts with the fact that $(\lambda^\star, P^\star_{\mathrm{Tx}})$ is the optimal solution. ■

With Lemma 2, problem (33) can be rewritten as

$$\min_{\lambda, P_{\mathrm{Tx}}} \ \lambda(1-p_o)\big(c_{\mathrm{BS}} + c_{\mathrm{Pw}}(P_{\mathrm{Tx}} + P_{\mathrm{C}})\big) \tag{35}$$

$$\text{s.t. } \overline{p}_c(l, w, p_o, \lambda, R) = \zeta_{\mathrm{Con}}, \tag{36}$$

$$R = f^{-1}(P_{\mathrm{Tx}}, P_{\mathrm{Th}}),$$

$$\lambda > 0, \quad 0 < P_{\mathrm{Tx}} \leq P^{\mathrm{Max}}_{\mathrm{Tx}},$$

which is non-convex due to the nonlinear equality constraint (36). Since $\overline{p}_c(l, w, p_o, \lambda, R)$ (i.e., $\overline{p}_{U_o}(l, w, p_o, \lambda, R)$ in (30)) is an implicit function of the λ and R, as Remark 2, a feasible pair (λ, R) satisfying $\overline{p}_c(l, w, p_o, \lambda, R) = \zeta_{\mathrm{Con}}$ can only be found by fixing one variable and searching for the other. The problem (35) has infinite feasible pairs of (λ, R), and it is challenging to efficiently find the optimal solution using existing monotonic optimization techniques. In the next subsection, by exploiting the derivations of $\overline{p}_{U_o}(l, w, p_o, \lambda, R)$ in (30), we propose a low-complexity search algorithm that finds the global optimal solution of problem (35).

B. OPTIMAL SEARCH ALGORITHM

The algorithm is designed based on the Remark 2. Note that BS coverage radius R is a real number, while variables determined by the R during computations of the $\overline{p}_{U_o}(l, w, p_o, \lambda, R)$ in set

$$\Upsilon = \left\{N^{\mathrm{LB}}_{\mathrm{Row}}, N^{\mathrm{UB}}_{\mathrm{Row}}, N^{\mathrm{LB}}_{\mathrm{Col}}, N^{\mathrm{UB}}_{\mathrm{Col}}, \alpha^{(i)}_b, \ \forall b, i \in [1, 4]\right\} \tag{37}$$

are all integers. These integers increase as R grows. However, according to (8) and (26), if R changes with a small extent, all integers in Υ can keep unchanged, resulting in the unchanged $\overline{p}_c(l, w, p_o, \lambda, R)$. In this way, we can partition the interval of BS coverage radius $0 < R \leq R^{\mathrm{Max}}$ into numerous subintervals. In each subinterval, all values of the R yield the same Υ in (37), and the minimum R corresponds to the smallest transmit power in (4). We collect the minimum R in each subinterval into a set $\mathcal{R}$. Obviously, the optimal BS coverage radius must be in the set $\mathcal{R}$. For each $R \in \mathcal{R}$, the λ guaranteeing $\overline{p}_c(l, w, p_o, \lambda, R) = \zeta_{\mathrm{Con}}$ can be found using the Bisection method [33]. By doing so, we obtain countable feasible pairs of $(\lambda, P_{\mathrm{Tx}})$. The one yielding the minimum objective function value in (35) is deemed as the optimal solution.

The set $\mathcal{R}$ is determined using Algorithm 1. In the algorithm, value of the t should be properly set. If t is larger than

[2]The period can be a number of hours, e.g., K hours, in which the installed BS is operating. If the power consumption cost for 1 Watt per hour is x, we have $c_{\mathrm{Pw}} = Kx$.

the range of a subinterval, the increment of R at step 3 may skip the subinterval, and the minimum R in this subinterval is not included in the $\mathcal{R}$. Besides, a large t will lead to non-negligible bias between the obtained values in $\mathcal{R}$ and true values of the minimum R in each subinterval. To avoid the above issues, the t should be small enough. However, a too small value of t may negatively affect the algorithm efficiency.

We now quantitatively show an appropriately value for t. According to (8) and (26), integers in Υ in (37) are used to describe the number of grids inside the boundary of the disk $\mathcal{O}(R)$. Since R in different subinterval have different Υ, the range of a subinterval should have the magnitude order similar to sizes of grids. We intuitively set the increment

$$t = 0.02 \min(l, w). \tag{38}$$

Since t in (38) can be large when both l and w are large, we further limit $t \leq 0.2$ and finally have

$$t = \min\left(0.02 \min(l, w), 0.2\right).$$

Algorithm 1

1: **given** $\mathcal{R} = \{0.1\}$, iteration index $i = 1$, step t.
2: Set $R = 0.1$ and compute $\Upsilon(i)$ in (37).
3: **for** $R = 0.1 + t : t : R^{\text{Max}}$ **do**
4: $\quad i = i + 1$.
5: $\quad$ Compute $\Upsilon(i)$ in (37).
6: $\quad$ **if** $\Upsilon(i) \neq \Upsilon(i-1)$ **then**
7: $\quad\quad \mathcal{R} = \mathcal{R} \cup R$.
8: $\quad$ **end if**
9: **end for**

Overhead of Algorithm 1 is low due to the limited iteration number R^{Max}/t and low-complexity step 5. To implement the Bisection method for each $R \in \mathcal{R}$, one should first find λ^{UB} and λ^{LB} satisfying

$$\overline{p}_c\left(l, w, p_o, \lambda^{\text{UB}}, R\right) > \zeta_{\text{Con}}, \quad \overline{p}_c\left(l, w, p_o, \lambda^{\text{LB}}, R\right) < \zeta_{\text{Con}}.$$

With the error tolerance ϵ, the number of iterations in the Bisection method for each $R \in \mathcal{R}$ is given by $\log\left((\lambda^{\text{UB}} - \lambda^{\text{LB}})/\epsilon\right)$ [33]. In each iteration, we compute the $\overline{p}_c\left(l, w, p_o, \lambda, R\right)$ once. In total, it is computed

$$|\mathcal{R}| \log\left((\lambda^{\text{UB}} - \lambda^{\text{LB}})/\epsilon\right)$$

times, where $|\mathcal{R}|$ is the cardinality of set $\mathcal{R}$.

While computing the $\overline{p}_c\left(l, w, p_o, \lambda, R\right)$, we need to compute the $\overline{p}^{(i)}_{\text{U}_o|\mathcal{C}_j}\left(l, w, p_o, \lambda, R\right), \forall i \in [1, 4]$ for J in (18) times. Seen from (29), complexity of $\overline{p}^{(i)}_{\text{U}_o|\mathcal{C}}\left(l, w, p_o, \lambda, R\right)$ is dominated by $\prod_{b=1}^{\eta_{+x}} \min\left(n_0^{(1)}, \alpha_b^{(i)}\right)$, which is huge when $n_0^{(1)} = \eta_{+y}$, η_{+x}, and $\alpha_b^{(i)}$ are large. In what follows, we focus on reducing the computational overhead of the $\overline{p}^{(i)}_{\text{U}_o|\mathcal{C}}\left(l, w, p_o, \lambda, R\right)$ in the case of huge $\prod_{b=1}^{\eta_{+x}} \min\left(n_0^{(1)}, \alpha_b^{(i)}\right)$.

C. ALGORITHM COMPLEXITY REDUCTION

Taking $\overline{p}^{(1)}_{\text{U}_o|\mathcal{C}}\left(l, w, p_o, \lambda, R\right)$ in (29) as the example, we reduce its complexity by shrinking the $\min\left(\alpha_b^{(1)}, n_{b-1}^{(1)}\right)$ in (29) into

$$\min\left(\alpha_b^{(1)}, n_{b-1}^{(1)}, \vartheta\right), \quad \forall b \in [1, \eta_{+x}], \tag{39}$$

where $\vartheta > 0$ is a newly introduced small integer. The $\Pr\left(\mathcal{N}^{(1)}\right)$ in (29) can be directly computed in (31) by replacing the $\min\left(\alpha_b^{(1)}, n_{b-1}^{(1)}\right)$ in (32) with $\min\left(\alpha_b^{(1)}, n_{b-1}^{(1)}, \vartheta\right)$. In this way, the complexity of $\overline{p}^{(1)}_{\text{U}_o|\mathcal{C}}\left(l, w, p_o, \lambda, R\right)$ is dominated by

$$\prod_{b=1}^{\eta_{+x}} \min(n_0^{(1)}, \alpha_b^{(1)}, \vartheta).$$

The ϑ should be properly selected. If ϑ is critically small, there are a few elements in $\{\Omega^{(1)}_{t|\mathcal{C}}\}_{t=1}^{T}$, and the $\overline{p}^{(1)}_{\text{U}_o|\mathcal{C}}\left(l, w, p_o, \lambda, R\right)$ in (29) will become to be a loose lower bound. On the other hand, large ϑ will nullify the computational reduction efforts because of

$$\min\left(\alpha_b^{(1)}, n_{b-1}^{(1)}\right) = \min\left(\alpha_b^{(1)}, n_{b-1}^{(1)}, \vartheta\right), \ \forall b \in [1, \eta_{+x}].$$

In this work, Algorithm 2 is designed to determine the ϑ that achieves a tradeoff between the lower bound tightness and complexity. In the algorithm, we initialize $\vartheta = 1$ and then gradually increase it. The increment of ϑ terminates when: (i) The computational time of the overall connectivity lower bound $\overline{p}_c\left(l, w, p_o, \lambda, R\right)$ exceeds a predefined threshold Γ^{Max}, or (ii) The increment of $\overline{p}_c\left(l, w, p_o, \lambda, R\right)$ from the previous iteration is smaller than a tolerance threshold $\epsilon > 0$. By integrating the Algorithm 2 into the above Bisection method, we finally obtain a low-complexity search algorithm.

Algorithm 2

1: **given** $\vartheta = 1$, tolerance $\epsilon = 10^{-3}$, maximum allowed computational time Γ^{Max}.
2: Regard ϑ as a variable for $\overline{p}_c\left(l, w, p_o, \lambda, R\right)$ and compute $\overline{p}_c\left(l, w, p_o, \lambda, R, \vartheta\right)$.
3: **while** 1 **do**
4: $\quad \vartheta = \vartheta + 1$.
5: $\quad$ Compute $\overline{p}_c\left(l, w, p_o, \lambda, R, \vartheta\right)$ and count the computational time Γ.
6: $\quad$ **if** $\Gamma > \Gamma^{\text{Max}}$ or $\overline{p}_c\left(l, w, p_o, \lambda, R, \vartheta\right) - \overline{p}_c\left(l, w, p_o, \lambda, R, \vartheta - 1\right) \leq \epsilon$ **then**
7: $\quad\quad \vartheta = \vartheta - 1$.
8: $\quad\quad$ Break.
9: $\quad$ **end if**
10: **end while**
11: **return** ϑ.

V. SIMULATION STUDIES

Numerical results are presented to verify the connectivity analysis and evaluate the BS deployment strategy. In the

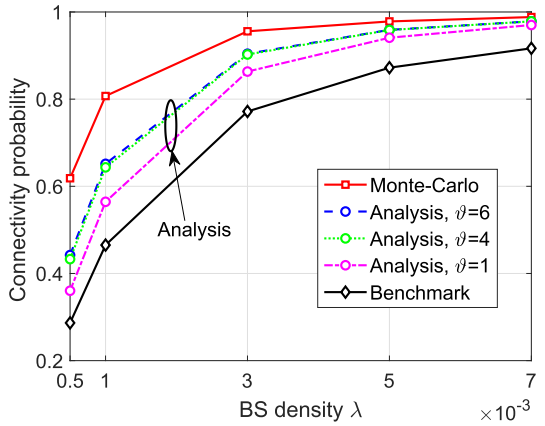

FIGURE 6. Connectivity lower bound $\overline{p}_c\,(l, w, p_o, \lambda, R)$ versus BS density λ under different ϑ with $p_o = 0.4$ and $R = 120$.

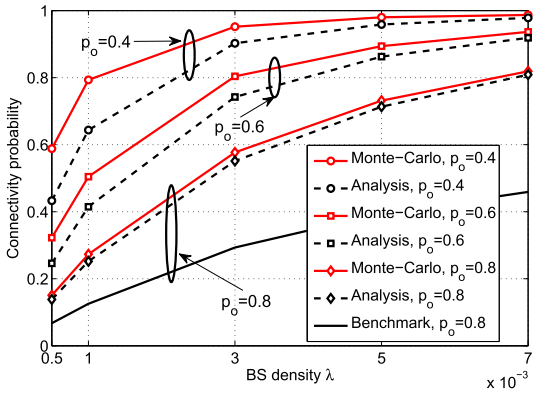

FIGURE 7. Connectivity lower bound $\overline{p}_c\,(l, w, p_o, \lambda, R)$ versus BS density λ under different p_o with $\vartheta = 5$ and $R = 120$.

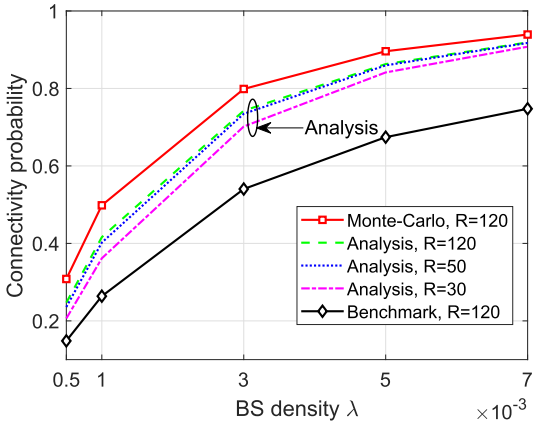

FIGURE 8. Connectivity probability $\overline{p}_c\,(l, w, p_o, \lambda, R)$ versus BS density λ under different R for $p_o = 0.6$ and $\vartheta = 5$.

connectivity comparison, lower bounds in [23] are taken as benchmarks. Throughout this section, the length and width of each grid are set to be $l = 15$ m and $w = 10$ m, respectively unless stated otherwise.

A. NETWORK CONNECTIVITY

In Algorithm 2, we know larger ϑ can yield tighter connectivity lower bound $\overline{p}_c\,(l, w, p_o, \lambda, R)$. We now quantitatively evaluate the impact of ϑ on the $\overline{p}_c\,(l, w, p_o, \lambda, R)$. Fig. 6 displays the $\overline{p}_c\,(l, w, p_o, \lambda, R)$ versus BS density λ under different ϑ for $p_o = 0.4$ and $R = 120$ m. For large λ, the analytical connectivity is close to that of Monte-Carlo simulation in even small ϑ. This is because large λ guarantees

$$1 - e^{-\lambda S\left(\Psi^{(1)}_{m|\mathcal{C}}\right)} \approx 1 - e^{-\lambda S\left(\Omega^{(1)}_{t_m|\mathcal{C}}\right)} \approx 1 \tag{40}$$

in (21) and (23) even though $S\left(\Psi^{(1)}_{m|\mathcal{C}}\right) - S\left(\Omega^{(1)}_{t_m|\mathcal{C}}\right)$ is large. This is to say, the lower bound in (23) is tight even though each $\Psi^{(1)}_{m|\mathcal{C}}$ is not accurately approximated by its maximum inscribed BFR. When ϑ is already large, increasing ϑ contributes little to tightness of the derived lower bound. This explains why gaps between the curves with $\vartheta = 4$ and $\vartheta = 6$ are minor. Seen from Fig. 6, $\vartheta = 5$ is enough to obtain a tight connectivity lower bound. Since $\vartheta = 5$ is not significantly large, the computational complexity of $\overline{p}_c\,(l, w, p_o, \lambda, R)$ is relatively low.

Fixing $\vartheta = 5$ and $R = 120$ m, we evaluate the connectivity lower bound $\overline{p}_c\,(l, w, p_o, \lambda, R)$ versus BS density λ with different p_o. As shown in Fig. 7, the connectivity lower bound $\overline{p}_c\,(l, w, p_o, \lambda, R)$ becomes critically tight when p_o is relatively large. This is because, in large obstacle occupation probability p_o, the connectivity $p^{(1)}_{\mathrm{U}_o|\mathcal{C}}$ in (21) is dominated by the instances of $\Psi^{(1)}$ with small areas. These small-area $\Psi^{(1)}_{m|\mathcal{C}}$s are usually close to their common region $\overline{\mathcal{C}}^{(1)}$ in (25) and thus can be well approximated by our derived BFR set in (25). In practical urban scenarios, the obstacle density is usually high, leading to relatively large p_o. Hence, our derived connectivity lower bound can be tight in mmWave MTG.

Setting $\vartheta = 5$ and $p_o = 0.6$, we show the connectivity lower bound $\overline{p}_c\,(l, w, p_o, \lambda, R)$ versus the BS density λ for different coverage radius R in Fig. 8. It is observed that, when R is relatively large, e.g., $R = 50$ m, increasing R (increasing transmit power) contributes little to the network connectivity. It means connectivity of an outdoor UE is mainly contributed by nearby BSs. This is due to the physical blockage, which is severe when path length is large. Compared to Monte-Carlo simulations, our derived connectivity lower bounds show great tightness, and the maximum bias is around 8%. This significantly outperforms the benchmark, whose offset can be over 20%. Seen from Fig. 8, the connectivity lower bound is monotonically increasing with respect to the BS density λ and coverage radius R.

The effect of different obstacle sizes on the network connectivity lower bound $\overline{p}_c\,(l, w, p_o, \lambda, R)$ is investigated in Fig. 9 under $p_o = 0.6$, $R = 100$, and $\vartheta = 5$. It is observed that increasing sizes of grids will dramatically improve the $\overline{p}_c\,(l, w, p_o, \lambda, R)$. It is due to the fact that larger l and w will result in fewer number of grids in $\mathcal{O}(R)$. Given the obstacle occupation probability p_o, it is easier to obtain BFR $\Psi^{(1)}$ in (16) with large area, which benefits the connectivity.

B. BASE STATION DEPLOYMENT

We evaluate the BS deployment strategy under $\vartheta = 5$ and $p_0 = 0.6$. For link budget in (3), we set the beam gain $G_{\mathrm{Tx}} = G_{\mathrm{Rx}} = 13$ dB, and power successful detection threshold

TABLE 1. Optimal solution of problem (35).

$c_{\mathrm{BS}}/c_{\mathrm{Pw}}$	1/40		1/1		40/1	
Connectivity threshold ζ_{Con}	0.8	0.9	0.8	0.9	0.8	0.9
$(\lambda^\star, R^\star)$	(0.0038,40.5)	(0.0062,40.5)	(0.0038,40.5)	(0.0062,40.5)	(0.0037,54.8)	(0.0060,54.8)
Monte-Carlo Connectivity	0.84	0.916	0.839	0.92	0.824	0.918

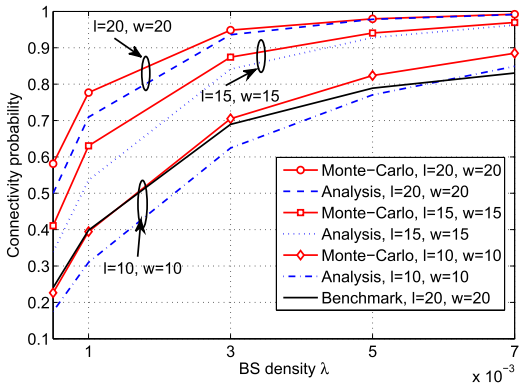

FIGURE 9. Connectivity probability $\bar{p}_c(l, w, p_o, \lambda, R)$ versus BS density λ under different obstacle length l and width w for $R = 100$, $p_o = 0.6$, and $\vartheta = 5$.

$P_{\mathrm{Th}} = -75$ dB. The constant circuit power consumption $P_{\mathrm{C}} = 3$ Watt in (35). Since problem (35) has the same optimal solution when the cost ratio $c_{\mathrm{BS}}/c_{\mathrm{Pw}}$ is fixed, we evaluate the results in different $c_{\mathrm{BS}}/c_{\mathrm{Pw}}$s: (i) $c_{\mathrm{BS}}/c_{\mathrm{Pw}} = 1/40$, (ii) $c_{\mathrm{BS}}/c_{\mathrm{Pw}} = 1/1$, and (iii) $c_{\mathrm{BS}}/c_{\mathrm{Pw}} = 40/1$. By solving problem (35), we obtain the optimal BS density and coverage radius tradeoff $(\lambda^\star, R^\star)$s and present them in TABLE 1.

Seen from TABLE 1, under the same connectivity threshold ζ_{Con}, the optimal BS coverage radius $R^\star$ increases as the power cost decreases. When the power cost is relatively low, e.g., $c_{\mathrm{BS}}/c_{\mathrm{Pw}} = 40/1$, the optimal BS coverage $R^\star$ approaches to its maximum value 54.8, observed from Fig. 8. In this situation, the increased connectivity threshold ζ_{Con} from 0.8 to 0.9 is contributed by increasing the BS density. In $c_{\mathrm{BS}}/c_{\mathrm{Pw}} = 1/40$ where power cost is relatively high, the BS coverage radius is smaller than its maximum value 54.8. To satisfy the increased connectivity threshold ζ_{Con}, increasing BS density is a more economical approach. We evaluate the network connectivity under the obtained $(\lambda^\star, R^\star)$ in Monte-Carlo simulations and append the connectivity probability in TABLE 1. Due to the tightness of our derived connectivity lower bound, the Monte-Carlo connectivity probabilities are close to the threshold ζ_{Con}.

VI. CONCLUSION

We devise a connectivity-constrained BS deployment strategy in the urban mmWave MTG modeled by random lattice process. This strategy finds the optimal tradeoff between the BS density and transmit power that minimizes the overall BS deployment cost. To mathematically formulate the problem, we devise a new analytical model to find a tight connectivity lower bound. Using the lower bound, we formulate the minimum cost BS deployment problem and optimally solve it by proposing a low-complexity search algorithm. The correctness and tightness of the analytical connectivity models are verified by comparing with the Monte-Carlo and existing benchmarks. The parameters impacting the connectivity probability are discussed, and BS deployment results are evaluated under different deployment cost settings.

VII. APPENDIX

Proof: According to (28), elements in $\mathcal{N}^{(1)}$ in (27) has the Markov property, i.e,.

$$\Pr\left(n_b^{(1)}|n_{b-1}^{(1)}, \ldots, n_0^{(1)}\right) = \Pr\left(n_b^{(1)}|n_{b-1}^{(1)}\right).$$

On this basis, the $\Pr(\mathcal{N}^{(1)})$ can be written into (31),

$$\begin{aligned}\Pr\left(\mathcal{N}^{(1)}\right) &= \Pr\left(n_0^{(1)}\right)\prod_{b=1}^{\eta_{+x}}\Pr\left(n_b^{(1)}|n_{b-1}^{(1)}, \ldots, n_0^{(1)}\right)\\ &= \prod_{b=1}^{\eta_{+x}}\Pr\left(n_b^{(1)}|n_{b-1}^{(1)}\right),\end{aligned}$$

where $\Pr\left(n_0^{(1)} = \eta_{+y}\right) = 1$ conditioned on a realization of $\mathcal{C}$ in (11). Deriving closed-form expression of the $\Pr\left(n_b^{(1)}|n_{b-1}^{(1)}\right)$ for $b \in [1, \eta_{+x}]$ is now of interest.

The $n_{b-1}^{(1)}$ determines domain of $n_b^{(1)}$, i.e.,

$$n_b^{(1)} \in \left[0, \min\left(\alpha_b^{(1)}, n_{b-1}^{(1)}\right)\right], \tag{41}$$

and $\Pr\left(n_b^{(1)}|n_{b-1}^{(1)}\right)$ is the probability that a $n_b^{(1)}$ is selected in the domain to guarantee the constraint $\sum_{a=1}^{n_b^{(1)}} z_{(a,b)} = 0$ at column b. Hence, we focus on the occupation state $z_{(a,b)}$s for $a \in [1, N_{\mathrm{Row}}]$.

When $n_b^{(1)} = \min(\alpha_b^{(1)}, n_{b-1}^{(1)})$ in (41), we have $z_{(a,b)} = 0$ for $a \in [1, n_b^{(1)}]$, and $z_{(a,b)}, \forall a \in [n_b^{(1)} + 1, N_{\mathrm{Row}}]$ can be in any value, yielding

$$\Pr\left(n_b^{(1)}|n_{b-1}^{(1)}\right) = (1 - p_o)^{n_b^{(1)}}.$$

When $n_b^{(1)} < \min(\alpha_b^{(1)}, n_{b-1}^{(1)})$, the $z_{(a,b)} = 0$ for $a \in [1, n_b^{(1)}]$, the $z_{(n_b^{(1)}+1,b)} = 1$, and $z_{(a,b)}, \forall a \in [n_b^{(1)} + 2, N_{\mathrm{Row}}]$ can be in any value, i.e.,

$$\Pr\left(n_b^{(1)}|n_{b-1}^{(1)}\right) = (1 - p_o)^{n_b^{(1)}} p_o.$$

Overall, we have the $\Pr\left(n_b^{(1)}|n_{b-1}^{(1)}\right)$ in (32). ■

REFERENCES

[1] S. Hur, T. Kim, D. J. Love, J. V. Krogmeier, T. A. Thomas, and A. Ghosh, "Millimeter wave beamforming for wireless backhaul and access in small cell networks," *IEEE Trans. Commun.*, vol. 61, no. 10, pp. 4391–4403, Oct. 2013.

[2] N. Gonzalez-Prelcic, A. Ali, V. Va, and R. W. Heath, Jr., "Millimeter-wave communication with out-of-band information," *IEEE Commun. Mag.*, vol. 55, no. 12, pp. 140–146, Dec. 2017.

[3] Z. Xiao, L. Zhu, J. Choi, P. Xia, and X.-G. Xia, "Joint power allocation and beamforming for non-orthogonal multiple access (NOMA) in 5G millimeter wave communications," *IEEE Trans. Wireless Commun.*, vol. 17, no. 5, pp. 2961–2974, May 2018.

[4] M. Dong, W.-M. Chan, T. Kim, K. Liu, H. Huang, and G. Wang, "Simulation study on millimeter wave 3D beamforming systems in urban outdoor multi-cell scenarios using 3D ray tracing," in *Proc. IEEE 26th Annu. Int. Symp. Pers., Indoor, Mobile Radio Commun. (PIMRC)*, Aug./Sep. 2015, pp. 2265–2270.

[5] W. Zhang, T. Kim, D. J. Love, and E. Perrins, "Leveraging the restricted isometry property: Improved low-rank subspace decomposition for hybrid millimeter-wave systems," *IEEE Trans. Commun.*, vol. 66, no. 11, pp. 5814–5827, Nov. 2018.

[6] L. Zhu, J. Zhang, Z. Xiao, X. Cao, D. O. Wu, and X. Xia, "Millimeter-wave NOMA with user grouping, power allocation and hybrid beamforming," *IEEE Trans. Wireless Commun.*, to be published.

[7] H. S. Ghadikolaei and C. Fischione, "Millimeter wave ad hoc networks: Noise-limited or interference-limited?" 2015, *arXiv:1509.04172*. [Online]. Available: https://arxiv.org/abs/1509.04172

[8] J. Choi, "On the macro diversity with multiple BSs to mitigate blockage in millimeter-wave communications," *IEEE Commun. Lett.*, vol. 18, no. 9, pp. 1653–1656, Sep. 2014.

[9] A. K. Gupta, J. G. Andrews, and R. W. Heath Jr., "Macro diversity in cellular networks with random blockages," 2017, *arXiv:1701.02044*. [Online]. Available: https://arxiv.org/abs/1701.02044

[10] J. G. Andrews, F. Baccelli, and R. K. Ganti, "A tractable approach to coverage and rate in cellular networks," *IEEE Trans. Commun.*, vol. 59, no. 11, pp. 3122–3134, Nov. 2011.

[11] M. Dong and T. Kim, "Interference analysis for millimeter-wave networks with geometry-dependent first-order reflections," *IEEE Trans. Veh. Technol.*, vol. 67, no. 12, pp. 12404–12409, Dec. 2018.

[12] H. Shokri-Ghadikolaei and C. Fischione, "The transitional behavior of interference in millimeter wave networks and its impact on medium access control," *IEEE Trans. Commun.*, vol. 64, no. 2, pp. 723–740, Feb. 2016.

[13] V. Petrov, M. Komarov, D. Moltchanov, J. M. Jornet, and Y. Koucheryavy, "Interference and SINR in millimeter wave and terahertz communication systems with blocking and directional antennas," *IEEE Trans. Wireless Commun.*, vol. 16, no. 3, pp. 1791–1808, Mar. 2017.

[14] T. Bai, R. Vaze, and R. W. Heath, Jr., "Analysis of blockage effects on urban cellular networks," *IEEE Trans. Wireless Commun.*, vol. 13, no. 9, pp. 5070–5083, Sep. 2014.

[15] M. Dong and T. Kim, "Reliability of an urban millimeter wave communication link with first-order reflections," in *Proc. IEEE Global Commun. Conf. (GLOBECOM)*, Dec. 2016, pp. 1–6.

[16] S. Kusaladharma and C. Tellambura, "Interference and outage in random D2D networks under millimeter wave channels," in *Proc. IEEE Int. Conf. Commun. (ICC)*, May 2017, pp. 1–7.

[17] K. Belbase, Z. Zhang, H. Jiang, and C. Tellambura, "Coverage analysis of millimeter wave decode-and-forward networks with best relay selection," *IEEE Access*, vol. 6, pp. 22670–22683, 2018.

[18] H. Jung and I.-H. Lee, "Outage analysis of millimeter-wave wireless backhaul in the presence of blockage," *IEEE Commun. Lett.*, vol. 20, no. 11, pp. 2268–2271, Nov. 2016.

[19] S. G. Larew, T. A. Thomas, M. Cudak, and A. Ghosh, "Air interface design and ray tracing study for 5G millimeter wave communications," in *Proc. IEEE Globecom Workshops (GC Wkshps)*, Dec. 2013, pp. 117–122.

[20] V. Nurmela, A. Karttunen, and A. Roivainen. (2011). *Deliverable D1.4 METIS Channel Models*. [Online]. Available: https://metis2020.com/wp-content/uploads/deliverables/METIS_D1.4_v1.0.pdf

[21] S. Marano, F. Palmieri, and G. Franceschetti, "Statistical characterization of ray propagation in a random lattice," *J. Opt. Soc. Amer. A, Opt. Image Sci.*, vol. 16, no. 10, pp. 2459–2464, 1999.

[22] G. Franceschetti, S. Marano, and F. Palmieri, "Propagation without wave equation toward an urban area model," *IEEE Trans. Antennas Propag.*, vol. 47, no. 9, pp. 1393–1404, Sep. 1999.

[23] K. Han, Y. Cui, Y. Wu, and K. Huang, "The connectivity of millimeter wave networks in urban environments modeled using random lattices," *IEEE Trans. Wireless Commun.*, vol. 17, no. 5, pp. 3357–3372, May 2018.

[24] D. Tsilimantos, J.-M. Gorce, and E. Altman, "Stochastic analysis of energy savings with sleep mode in OFDMA wireless networks," in *Proc. IEEE INFOCOM*, Apr. 2013, pp. 1097–1105.

[25] D. Cao, S. Zhou, and Z. Niu, "Optimal base station density for energy-efficient heterogeneous cellular networks," in *Proc. IEEE Int. Conf. Commun. (ICC)*, Jun. 2012, pp. 4379–4383.

[26] D. Cao, S. Zhou, and Z. Niu, "Optimal combination of base station densities for energy-efficient two-tier heterogeneous cellular networks," *IEEE Trans. Wireless Commun.*, vol. 12, no. 9, pp. 4350–4362, Sep. 2013.

[27] J. Peng, P. Hong, and K. Xue, "Energy-aware cellular deployment strategy under coverage performance constraints," *IEEE Trans. Wireless Commun.*, vol. 14, no. 1, pp. 69–80, Jan. 2015.

[28] T. Zhang, J. Zhao, L. An, and D. Liu, "Energy efficiency of base station deployment in ultra dense HetNets: A stochastic geometry analysis," *IEEE Wireless Commun. Lett.*, vol. 5, no. 2, pp. 184–187, Apr. 2016.

[29] S. Chatterjee, M. J. Abdel-Rahman, and A. B. MacKenzie, "Optimal base station deployment with downlink rate coverage probability constraint," *IEEE Wireless Commun. Lett.*, vol. 7, no. 3, pp. 340–343, Jun. 2018.

[30] N. A. Muhammad, P. Wang, Y. Li, and B. Vucetic, "Analytical model for outdoor millimeter wave channels using geometry-based stochastic approach," *IEEE Trans. Veh. Technol.*, vol. 66, no. 2, pp. 912–926, Feb. 2017.

[31] T. Rappaport, Y. Xing, G. R. MacCartney, A. F. Molisch, E. Mellios, and J. Zhang, "Overview of millimeter wave communications for fifth-generation (5G) wireless networks-with a focus on propagation models," *IEEE Trans. Antennas Propag.*, vol. 65, no. 12, pp. 6213–6230, Dec. 2017.

[32] R. Tang, J. Cheng, and Z. Cao, "Energy-efficient power allocation for cooperative NOMA systems with IBFD-enabled two-way cognitive transmission," *IEEE Commun. Lett.*, vol. 23, no. 6, pp. 1101–1104, Jun. 2019.

[33] R. Burden and J. Faires. (2011). *Solutions of Equations in One Variable: The Bisection Method*. [Online]. Available: https://www.math.ust.hk/~mamu/courses/231/Slides/ch02_1.pdf

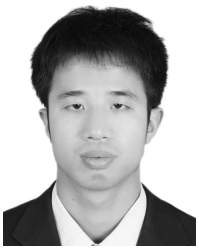

MIAOMIAO DONG received the B.Eng. degree from Northwestern Polytechnical University, China, in 2010, and the M.Eng. degree from Xidian University, in 2013, China. From 2013 to 2016, he was a Research Assistant with the City University of Hong Kong, where he is currently pursuing the Ph.D. degree. His research interests include millimeter wave channel modeling, millimeter wave network performance analysis, and precoder design in massive MIMO systems.

TAEJOON KIM (S'08–M'11) received the B.S. degree (Hons.) from Sogang University, in 2002, the M.S. degree from KAIST, in 2004, and the Ph.D. degree in electrical and computer engineering from Purdue University, West Lafayette, IN, USA, in 2011.

From 2011 to 2012, he was with the Nokia Research Center, Berkeley, CA, USA, as a Senior Researcher. Before joining The University of Kansas as an Assistant Professor, he was a Post-Doctoral Researcher with the KTH Royal Institute of Technology, Stockholm, Sweden, and an Assistant Professor with the City University of Hong Kong, from 2013 to 2017. He holds 26 issued U.S. patents. His research interests include design and analysis of communication systems, and statistical signal processing. He received the President's Award of the City University of Hong Kong, in 2017. He was a recipient of the IEEE PIMRC Best Paper Award, in 2012, the Nokia Research Center Kudos Award, in 2012, and the IEEE Communications Society Stephen O. Rice Prize, in 2016. Since 2016, he has been served as an Associate Editor of the IEEE TRANSACTIONS ON COMMUNICATIONS.

JINGJIN WU received the B.Eng. degree (Hons.) in information engineering (with finance minor), in 2011, and the Ph.D. degree in electronics engineering from the City University of Hong Kong, Hong Kong, in 2016. Since 2016, he has been an Assistant Professor with the Statistics Department, BNU–HKBU United International College, China. His current research interests include performance evaluation and energy conservation of cellular networks.

ERIC W. M. WONG received the B.Sc. and M.Phil. degrees in electronic engineering from The Chinese University of Hong Kong, in 1988 and 1990, respectively, and the Ph.D. degree in electrical and computer engineering from the University of Massachusetts at Amherst, in 1994. He joined the Department of Electrical Engineering, City University of Hong Kong, in 1994. His current research interests include analysis and design of telecommunications networks, optical networks, and cellular networks. He served as a Guest Editor for the IEEE JOURNAL ON SELECTED AREAS IN COMMUNICATIONS–one of the highest ranked journals in the field of telecommunications–for the special issue Next Generation Spectrum-Efficient and Elastic Optical Transport Networks.